Electronic Supplementary Material (ESI) for Nanoscale.

SUPPLEMENTAL INFORMATION

Surface functionalization of gold nanoclusters with arginine: A trade-off between microtumor uptake and radiotherapy enhancement

Mans Broekgaarden *[a], Anne-Laure Bulin [b], Estelle Porret [a], Benjamin Musnier [a], Benoit Chovelon [c,d], Corinne Ravelet [c], Lucie Sancey [a], Hélène Elleaume [b], Pierre Hainaut [a], Jean-Luc Coll *[a], Xavier Le Guével[a]

[a.] *Institute for Advanced Biosciences, Université Grenoble-Alpes, INSERM U1209, CNRS UMR5309, Allée des Alpes, 38700 La Tronche, France.*
[b.] *Synchrotron Radiation for Biomedicine, UA 07 INSERM (STROBE), Université Grenoble-Alpes, European Synchrotron Radiation Facility, 71 avenue des Martyrs CS40220, 38043 Grenoble, France.*
[c.] *Université Grenoble-Alpes, Département de Pharmacochimie Moléculaire UMR 5063, 470 rue de la Chimie, 38400 St Martin d'Hères, France.*
[d.] *Institut de Biologie et Pathologie, CHU de Grenoble-Alpes, 9 Boulevard de la Chantourne, 38700 La Tronche, France*
** Corresponding authors: mans.broekgaarden@univ-grenoble-alpes.fr;, jean-luc.coll@univ-grenoble-alpes.fr*

Experimental

Synthesis of AuNCs

Arginine modified-glutathione peptides SG-2Arg = $C_{22}H_{4}0N_{11}O_{8}S$ $(CF_3COO-)_2$ with 10 % of H_2O and purity ≥ 95% were purchased from GenScript (Piscataway, NJ, USA). Gold(III)chloride trihydrate ($HAuCl_4{\cdot}3H_2O$, reagent grade), reduced L-glutathione ($C_{10}H_{17}N_3O_6S$, ≥98%) sodium borohydride ($NaBH_4$) and isopropyl alcohol (99%) were purchased from Sigma-Aldrich (Saint-Quentin-Fallavier, France). Sodium hydroxide (NaOH, 98%) and hydrochloric acid (HCl, 35−37%), were purchased from Laurylab (Brindas, France) and VWR Chemicals (Fontenay-sous-Bois, France). All the chemicals were used as received without further purification. Water was purified using a Millipore Milli-Q system (Millipore, France).

The synthesis was achieved by adapting the protocol described by *Pyo et al.* [1] to produce $Au_{22}SG_{18}$. In our case the molar ratio Au:SG/SG-2Arg was 1:1.5. Therefore, 48 mg of SG or 145.7 mg of SG-2Arg was dissolved in 3 mL of water, followed by the addition of 5 mL of $HAuCl_4.3H_2O$ (20 mM) and 95 mL of distilled water. The pH was adjusted at 9 before the dropwise addition of the reducing agent $NaBH_4$ (5 mM, 250 µL, freshly prepared in cold water). The solution was stirred for 30 min and the pH maintained at 9. Then, the pH was decreased to 2 to stop the reduction process. To complete the reaction, the solution was stirred 4 more hours. Afterwards, the solution was rotary evaporated, re-solubilized in 10 mL of water and ~12 mL of isopropyl alcohol was added to precipitate the AuNCs. The AuNCs were collected by centrifugation and the supernatant was centrifuged twice to maximize the recovery of AuNCs. The AuNCs were re-solubilised in water and the pH was adjusted to 7, before to lyophilization. Immediately prior to use in cell culture exeriments, the AuNC powder was reconsituted in sterile phosphate buffered saline and filter sterilized.

Characterization of AuNCs

AuNC core sizes were determined using high resolution transmission electron microscopy (HR-TEM, JEOL 2010 LaB6 microscope, 200 kV, 0.19 nm point-to-point resolution), after the deposition of the AuNC (10 µL, 4 mg Au/mL) on a formvar carbon grid (Agar Scientific, Essex, UK). The hydrodynamic diameter (HD) of AuNCs (~2 mM, D2O, pH 7) was determined by diffusion ordered nuclear magnetic resonance spectroscopy (Bruker AVANCE III 500 MHz spectrometer, 298 K, Palaiseau, France). The experiments were run using the standard “ledbpg2s” Bruker sequence with linear gradient stepped between 2% and 98% and 32 scans for each gradient step. The average value of the diffusion coefficient D was obtained using the maximum entropy algorithm from the Dynamics Center software (Bruker, Palaiseau, France). The HD was calculated according to the Stokes-Einstein equation which assumes that molecules are spherical:

$$HD = k_BT/\ 3D\pi\eta$$

Here, k_B is the Boltzmann constant, T is the temperature, η is the viscosity of the solvent ($\eta D_2O = 1.232\ 10^{-3}$ Pa.s at 298 K). Absorption spectra between 400 and 900 nm were obtained using a Lambda 650 UV-VIS spectrophotometer (Perkin-Elmer), at a concentration of 0.4 mg Au/mL in PBS (10 mM). Photoluminescence spectra between 470 and 870 nm were determined using a Fluoromax-4 spectrofluorimeter (HERIBA Scientific) at a concentration of 0.04 mg Au/mL (~0.04 optical density) in PBS ($\lambda_{exc.}$= 450 nm). Zeta potential of the AuNCs (0.04 mg Au/mL) were measured in PBS (10 mM) using a Zetasizer (Malvern Panalytical, Malvern, UK). Measurements were performed in triplicate at 25°C using 1.34 for the refractive index, 1.1 mPa.s for the viscosity and 79.0 for the dielectric constant.

Cell cultures

The human U87MG glioblastoma cell line and rat F98 malignant glioma cell line were obtained from the American Type Culture Collection (Manassas, VA). Cell lines were maintained in DMEM containing 5 mM Glutamax (Gibco, ThermoFisher, St Herblain, France), supplemented with 10% fetal bovine serum (Gibco), 1% penicillin and streptomycin (Gibco). Cells were passaged weekly at a 1:10 ratio (U87MG), or a 1:20 ratio (F98). Cells were discarded upon reaching passage 30. Spheroids were initiated by seeding 2.5×10^3 cells U87MG and F98 cells in each well of 96-well U-bottom ultra-low attachment plates (Corning). Spheroids formed within 24h of culture.

Toxicity evaluation

Toxicity of the AuNCs in absence of further treatment was assessed in dose-escalation experiments. Three days-old glioblastoma spheroids were incubated with increasing doses (10-250 µg Au/mL) of AuNC and incubated for either 12 h (short term toxicity) or 96 h (long-term toxicity), after which viability was assessed using *in situ* 2 µM calcein AM (ThermoFisher) and 3 µM propidium iodide (Sigma-Aldrich) staining, followed by confocal laser scanning fluorescence microscopy (Zeiss LSM710, Marly le Roi, France). Spheroid size (growth effects), viability, and the extent of necrosis was quantified as described in the section *Multiparametric assessment of radiotherapy efficacy*, and as described previously [2].

For toxicity evaluations on non-malignant cells, human umbilical vein endothelial cells (HUVEC) and Met5A mesothelial cells were selected. Cells were seeded at a density of 10.000 cells per well in a 96-well plate, and reached confluence overnight.

AuNC uptake and localization

Glioblastoma spheroids were seeded on day 1. On day 3, the spheroids were incubated for 2 h, 12 h or 24 h with 100 µg Au/mL AuSG or AuSG-2Arg. After incubation, the spheroids were collected in microcentrifuge tubes, spun down, and washed three times with 1 mL PBS, and resuspended in final volume of 0.1 mL PBS. Uptake was then assessed using either confocal laser scanning NIR fluorescence microscopy, SWIR fluorescence imaging, or inductively coupled plasma mass spectrometry (ICP-MS).

For NIR and SWIR fluorescence imaging, the spheroid suspension was transferred to glass-bottom 24-well plates (Greiner Sensoplates, Sigma-Aldrich). For confocal fluorescence microscopy (Zeiss LSM710), the AuNCs were detected using $\lambda_{exc.}$ = 405 nm, $\lambda_{em.}$ = 600-800 nm. Image acquisition was conducted using a 20× air objective (NA 0.3), a resolution of 1024 × 1024 px, a z-resolution of 10 µm, and a scanning speed of 1.58 µs/px. Quantitative imaging was performed by minimizing signal detection on spheroids incubated in absence of AuNCs, while ensuring that no signal saturation occurred in the spheroids incubated with AuNCs. Image analysis was performed using a custom script in Matlab 2016b (Mathworks, Natick, MA) to extract median fluorescence intensities per organoid (as detailed in *Bulin et al.* [2]).

SWIR imaging was performed on a custom-built platform, using an 830 nm LED excitation source (60 mW/cm^2), and the fluorescence was collected between 1064-1700 nm (long-pass filter 1064 -Semrock), on a Nirvana 640 ST camera (Princeton) through a 25 mm lens (NA 1.4, Navitar). The exposure time was 2 s. Image analysis was performed using ImageJ (NIH, Bethesda MD) by taking the median intensity in manually defined regions of interest, drawn around the individual spheroids.

For ICP-MS, the spheroids were incubated with the AuNCs at the indicated timepoints, and 20-48 spheroids were pooled and transferred to microcentrifuge tubes, spun down, and washed three times with 1 mL PBS. Subsequently, spheroids were lysed in 1% (v/v) nitric acid (ultrapure Normaton, VWR, Leuven, Belgium), and measured using ICP-MS (X Serie II, Thermo Electron, Bremen, Germany) equipped with quartz impact bead spray chamber and concentric nebulizer. Standard solutions were prepared in nitric acid 1% (v/v). ^{197}Au was measured, and ^{103}Rh was used as internal standard.

Transmission electron microscopy

U87MG spheroids were established and treated as described in section *"AuNC uptake and localization"*. Immediately following 12h exposure to the AuNCs, the spheroids were collected and 8-12 spheroids were pooled per treatment group. The spheroids were fixed for 24 h in 2% paraformaldehyde, 0.2% glutaraldehyde in PBS. Subsequently, the spheroids were incubated for 1 h with 1% OsO_4 on ice, after which the spheroids we dehydrated with ice-cold ethanol. The spheroids were then embedded in epoxy resin. Following two days of solidification, the spheroids were sectioned and imaged on a JEOL 1200EX transmission electron microscope (Peabody MA, USA). We thank Dr. Karin Pernet-Gallay and Anne Bertrand (Grenoble Institute for Neurosciences) for facilitating the electron microscopy imaging.

Radiation therapy

Spheroid cultures were initiated on day 1 in a volume of 50 µL/well, and incubated with 100 µg Au/mL AuNCs on day 3 for a duration of 12 h (final volume 100 µl/well). Following incubation, spheroids were washed twice by the repetitive addition and aspiration of 100 µL culture medium, leaving a final volume of 200 µL culture medium in the wells. Plates were irradiated using monochromatic synchrotron radiation at the ID17 medical beamline (European Synchrotron Radiation Facility, Grenoble, France) at an energy of 50 keV, unless indicated otherwise. Spheroids received a final radiation dose ranging from 2-12 Gy. Spheroids were imaged every 2-3 days using brightfield microscopy (Zeiss AxioObserver Z1), and image analysis was performed using a custom-written script in Matlab 2016b (Mathworks, Natick, MA). Multiparametric assessment of treatment effects was performed on day 14 (see below).

Multiparametric assessment of radiotherapy efficacy

Spheroids were stained *in situ* with 2 µM calcein AM (ThermoFisher) and 3 µM propidium iodide (Sigma-Aldrich). Confocal laser scanning fluorescence microscopy (Zeiss LSM710) was done at 10x magnification (NA 0.3), scanning speed: 1.58 µs/px, an image size of 850.19 µm^2, a resolution of 0.602 px/µm, and an open pinhole to maximize signal collection. Quantitative automated image analysis for multiparametric assessment of treatment effects was done using the CALYPSO method [2]. In this study, the size, viability, and the extent of necrosis of the spheroids were used to evaluate treatment response, which was based on previous investigations [3].

Quantitative imaging of oxidative stress

Oxidative stress was quantified using dichlorodihydrofluorescein-diactetate (DCFH$_2$-DA), a fluorescent probe for oxidative stress [4,5]. DCFH$_2$-DA traverses cell membranes after which intracellular esterases entrap DCFH$_2$ inside the cytoplasm. Presence of oxidative species oxidize DCFH$_2$ to form the fluorescent DCF. In this assay, treated spheroids were incubated with 50 µM DCFH$_2$-DA (ThermoFisher) for 60 min (37°C, 5% CO$_2$) on culture days 8 and 14 (*i.e.*, 5 and 11 days post-treatment). Spheroids were then imaged with confocal laser scanning fluorescence microscopy (10× objective, NA 0.3, image size: 1414.2 µm^2, resolution: 0.602 px/µm, scanning speed: 1.58 µs/px, 176.6 µm focal plane). Images were analyzed with CALYPSO for automated DCF signal quantification.

To investigate how the AuNCs affect cellular redox states, U87MG and F98 cells were seeded in 96 wells plates at a density of 1 × 10^4 cells/well and allowed to reach confluence overnight. The cells were then incubated in PBS, and exposed to either AuSG (50µg/mL) or AuSG-2Arg (50µg/mL). PBS alone was selected as the negative control, whereas FBS (25%) was used as an antioxidant control. Immediately thereafter, the cells were exposed to a final concentration of 1mM ammonium ferrous sulfate ($(NH_4)_2Fe^{(II)}(SO_4)_2(H_2O)_6$) (Sigma-Aldrich). The presence of ferrous iron in biological media is known to catalyze the production of various ROS, most notably OH$_2$, H$_2$O$_2$, and $^\bullet$OH which is relevant to radiotherapy [6]. Upon starting the incubation with Fe^{2+}, oxidative stress was measured by the addition of 25µM DCFH$_2$-DA to the cells. The fluorescence of its oxidation product DCF was measured at λ_{ex} = 485 nm and λ_{em} = 520 nm (FluoStar Omega plate reader, BMG Labtech, Champigny-sur-Marne, France).

Statistical analysis

All statistical analyses were performed in Graphpad Prism 5.0 (La Jolla, CA). Data was assessed for normality, after which appropriate statistical tests were performed as indicated. Normally distributed data was analyzed using a one-way ANOVA and Bonferroni post-hoc test for multiple comparisons, or otherwise analyzed using a Kruskal-Wallis and Dunn's post-hoc test for multiple comparisons. Normalized dose response curves were fitted, and IC50/EC50 values were compared using an extra sum-of-squares F-test. The extent of statistical significance is indicated with either a single asterisk ($p \leq 0.05$), double asterisks ($p \leq 0.01$) or triple asterisks ($p \leq 0.005$).

Extended Discussion

Radiotherapy enhancement by AuNCs

The ability of AuNCs to enhance radiotherapy efficacy stems from at least two mechanisms. During radiotherapy, the presence of Au in tumor tissues can result in higher degrees of radiation absorption, after which the energy is locally deposited to enhance radiation-induced tissue damage by increased levels of $^\bullet$OH [7,8]. This radiation dose-enhancement effect is considered the main mechanism of increased radiotherapy efficacies in the orthovoltage (keV) range, as the absorption difference between Au and soft tissue diminishes at higher X-ray energies (MeV) [9]. Interestingly, most studies have been performed with energies at which this absorption difference is largely absent. For example, the studies by *Zhang et al.*, which clearly demonstrated a radiosensitization effect, were performed using a 662 keV X-ray source [10–12]. These findings suggest that alternative mechanisms of radiotherapy enhancement by Au exist [13,14]. Indeed, such effects have been attributed to a "chemical enhancement" mechanism, leading to the production of ROS and severe oxidative stress in cancer tissues [13–15]. Another theory suggests that radiosensitization with high Z-element particles may stem from nano-sized spots of intense radiation deposition around the particles, which can occur independently of the X-ray energy [16–18].

Models for evaluating theranostic AuNCs

Various studies have already been conducted to investigate radiation dose-enhancement by AuNCs, including the aforementioned studies by *Zhang et al.* [10–12]. Studies on novel AuNCs using 2D cultures by our group have often produced promising results that failed to be effectively translated to *in vivo* studies. This has been a major driving force for us and others to explore 3D culture models to better bridge the gap between *in vitro* and *in vivo* research. In addition, the use of 3D cultures for radiotherapy enhancement has only sporadically been explored. 2D cultures are relevant investigational models in case monolayers are representative to the *in vivo* manifestation of tissues, *e.g.*, monolayers of non-malignant (vascular) epithelial cells and mesothelial cells. However, when modeling cancer, 2D cultures are widely regarded as inferior models compared to 3D cultures. This is based on the facts that 2D monolayers do not mimic heterogeneous drug penetration [19], oxygen gradients [20], and drug resistance [21]. For example, a preliminary study on the synthesis and characterization of the of Arg-functionalized AuSG nanoclusters included uptake and toxicity assays on 2D cell cultures [22]. The uptake assays in 2D cultures demonstrated rapid uptake (<5min) and excretion (>30 min) of the AuSG-2Arg in COLO829 melanoma cells, whereas the uptake in glioblastoma spheroids peaked at 12h of incubation. Furthermore, a concentration of 100 μg/mL was found to induce significant toxicity in COLO829 monolayers following 24h exposure, whereas a similar treatment induced no noticeable toxicity after 96h of exposure in our glioblastoma spheroids. Lastly, *Naidu et al.*, published radiotherapy dose-response evaluations in 2D U87MG cells to demonstrate <10% cell survival at a 1Gy dose [23], whereas we show that a dose of 12Gy was incapable of reducing U87MG spheroid viability below 40%. *In vivo* radiotherapy studies on rats carrying orthotopic F98 glioblastoma have been performed with 3 fractions of 8 Gy, which only achieved a minor increase in overall survival [24]. This illustrates that treatment efficacies in 2D cultures can be off by a factor of 10-100 when compared to 3D/*in vivo* models of cancer. Thus, although 2D cultures are useful models for detailed investigation on the subcellular effects of cancer therapies, results on global therapeutic evaluations bear very little resemblance to those obtained in 3D culture models and *in vivo* models of cancer.

References

1 K. Pyo, V. D. Thanthirige, K. Kwak, P. Pandurangan, G. Ramakrishna and D. Lee, *J. Am. Chem. Soc.*, 2015, **137**, 8244–8250.
2 A.-L. Bulin, M. Broekgaarden and T. Hasan, *Sci Rep*, 2017, 16445.
3 A.-L. Bulin, M. Broekgaarden, D. Simeone and T. Hasan, *Oncotarget*, 2019, 2625–2643.
4 B. Kalyanaraman, V. Darley-Usmar, K. J. A. Davies, P. A. Dennery, H. J. Forman, M. B. Grisham, G. E. Mann, K. Moore, L. J. Roberts and H. Ischiropoulos, *Free Radic Biol Med*, 2012, **52**, 1–6.
5 M. J. Reiniers, R. F. van Golen, S. Bonnet, M. Broekgaarden, T. M. van Gulik, M. R. Egmond and M. Heger, *Anal. Chem.*, 2017, **89**, 3853–3857.
6 J. Weiss, *Naturwissenschaften*.
7 M. Misawa and J. Takahashi, *Nanomedicine*, 2011, **7**, 604–614.
8 J. D. Carter, N. N. Cheng, Y. Qu, G. D. Suarez and T. Guo, *J Phys Chem B*, 2007, **111**, 11622–11625.
9 J.-L. Ravanat and T. Douki, *Radiation Physics and Chemistry*, 2016, **128**, 92–102.
10 X.-D. Zhang, Z. Luo, J. Chen, X. Shen, S. Song, Y. Sun, S. Fan, F. Fan, D. T. Leong and J. Xie, *Adv. Mater. Weinheim*, 2014, **26**, 4565–4568.
11 X.-D. Zhang, Z. Luo, J. Chen, S. Song, X. Yuan, X. Shen, H. Wang, Y. Sun, K. Gao, L. Zhang, S. Fan, D. T. Leong, M. Guo and J. Xie, *Sci Rep*, 2015, **5**, 8669.
12 X.-D. Zhang, J. Chen, Z. Luo, D. Wu, X. Shen, S.-S. Song, Y.-M. Sun, P.-X. Liu, J. Zhao, S. Huo, S. Fan, F. Fan, X.-J. Liang and J. Xie, *Adv Healthc Mater*, 2014, **3**, 133–141.
13 K. T. Butterworth, S. J. McMahon, F. J. Currell and K. M. Prise, *Nanoscale*, 2012, **4**, 4830–4838.
14 L. Cui, S. Her, G. R. Borst, R. G. Bristow, D. A. Jaffray and C. Allen, *Radiother Oncol*, 2017, **124**, 344–356.
15 N. N. Cheng, Z. Starkewolf, R. A. Davidson, A. Sharmah, C. Lee, J. Lien and T. Guo, *J. Am. Chem. Soc.*, 2012, **134**, 1950–1953.
16 L. Sancey, F. Lux, S. Kotb, S. Roux, S. Dufort, A. Bianchi, Y. Crémillieux, P. Fries, J.-L. Coll, C. Rodriguez-Lafrasse, M. Janier, M. Dutreix, M. Barberi-Heyob, F. Boschetti, F. Denat, C. Louis, E. Porcel, S. Lacombe, G. Le Duc, E. Deutsch, J.-L. Perfettini, A. Detappe, C. Verry, R. Berbeco, K. T. Butterworth, S. J. McMahon, K. M. Prise, P. Perriat and O. Tillement, *The British Journal of Radiology*, 2014, **87**, 20140134.
17 E. Porcel, S. Liehn, H. Remita, N. Usami, K. Kobayashi, Y. Furusawa, C. Le Sech and S. Lacombe, *Nanotechnology*, 2010, **21**, 85103.
18 S. J. McMahon, W. B. Hyland, M. F. Muir, J. A. Coulter, S. Jain, K. T. Butterworth, G. Schettino, G. R. Dickson, A. R. Hounsell, J. M. O'Sullivan, K. M. Prise, D. G. Hirst and F. J. Currell, *Radiother Oncol*, 2011, **100**, 412–416.
19 R. A. Alderden, H. R. Mellor, S. Modok, M. D. Hall, S. R. Sutton, M. G. Newville, R. Callaghan and T. W. Hambley, *J. Am. Chem. Soc.*, 2007, **129**, 13400–13401.
20 L. G. Griffith and M. A. Swartz, *Nat. Rev. Mol. Cell Biol.*, 2006, **7**, 211–224.

21 W. D. Stein, T. Litman, T. Fojo and S. E. Bates, *Int. J. Cancer*, 2005, **113**, 861–865.
22 E. Porret, J.-B. Fleury, L. Sancey, M. Pezet, J.-L. Coll and X. Le Guével, *RSC Advances*.
23 M. D. Naidu, J. M. Mason, R. V. Pica, H. Fung and L. A. Peña, *J. Radiat. Res.*, 2010, **51**, 393–404.
24 J. Rousseau, C. Boudou, R. F. Barth, J. Balosso, F. Estève and H. Elleaume, *Clin. Cancer Res.*, 2007, **13**, 5195–5201.

Supplemental Figures

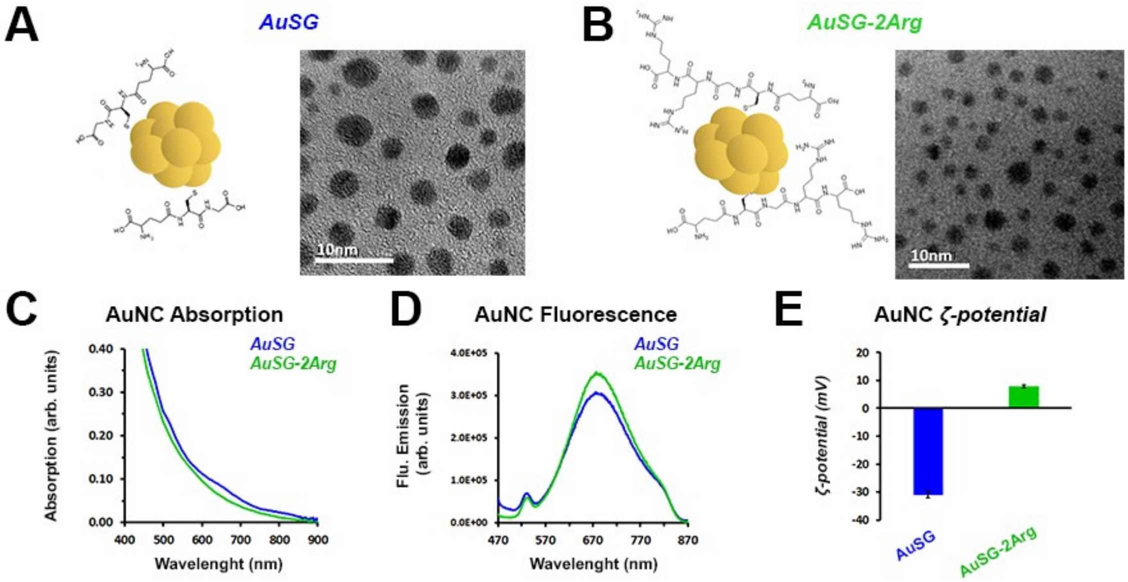

Figure S1. Characterization of the AuNCs. (A-B) Schematic overview and high resolution TEM images of AuSG and AuSG-2Arg. Absorption (C), Fluorescence (D; $\lambda_{exc.}$= 450 nm), and zeta potential (E) of AuSG (blue)and AuSG-2Arg (green) in water.

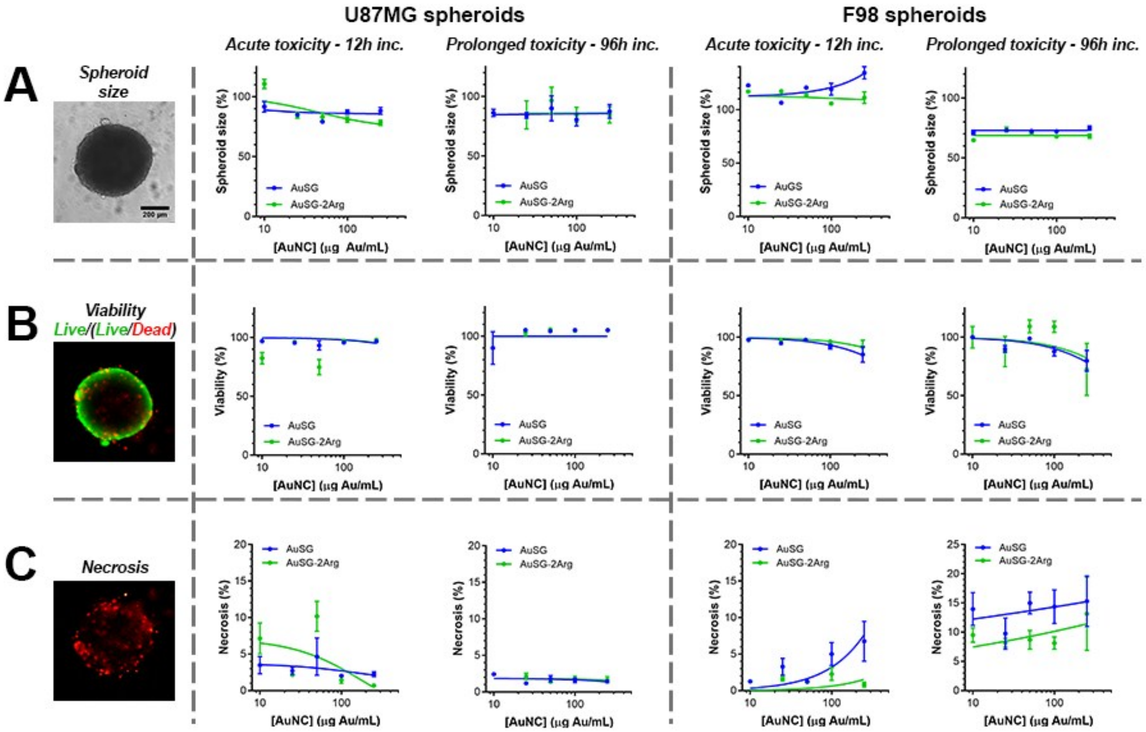

Figure S2. Acute and prolonged toxicity of AuNCs in glioblastoma spheroids. Quantification of spheroid size based on brightfield images (representative image shown on the left) **(A)**, viability calculated as the live signal (green)/(dead signal (red)+live signal) (representative image shown on the left). **(B)**, and necrosis (dead signal, red) (representative image shown on the left) **(C)** following a 12 h- or 96 h exposure to AuSG (blue) or AuSG-2Arg (green). Spheroid sizes and viabilities were normalized to the no treatment controls, whereas the necrosis data was indexed based on the total killing control (100% necrosis). All data represents the mean ± SEM (N = 3-6 from 2 technical repeats).

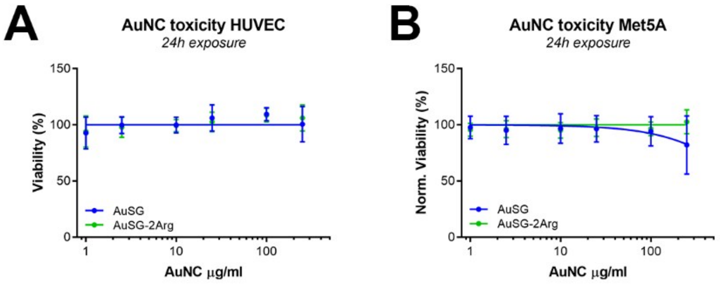

Figure S3. Toxicity evaluation of AuSG (blue) and AuSG-2Arg (green) on human non-malignant cell lines following 24h of exposure. (A) AuNC dose response curves on non-malignant HUVEC vascular endothelial cells. (B) AuNC dose response curves on non-malignant Met5A mesothelial cells. The results depict the mean±SD from N ≥ 9 from three technical repeats.

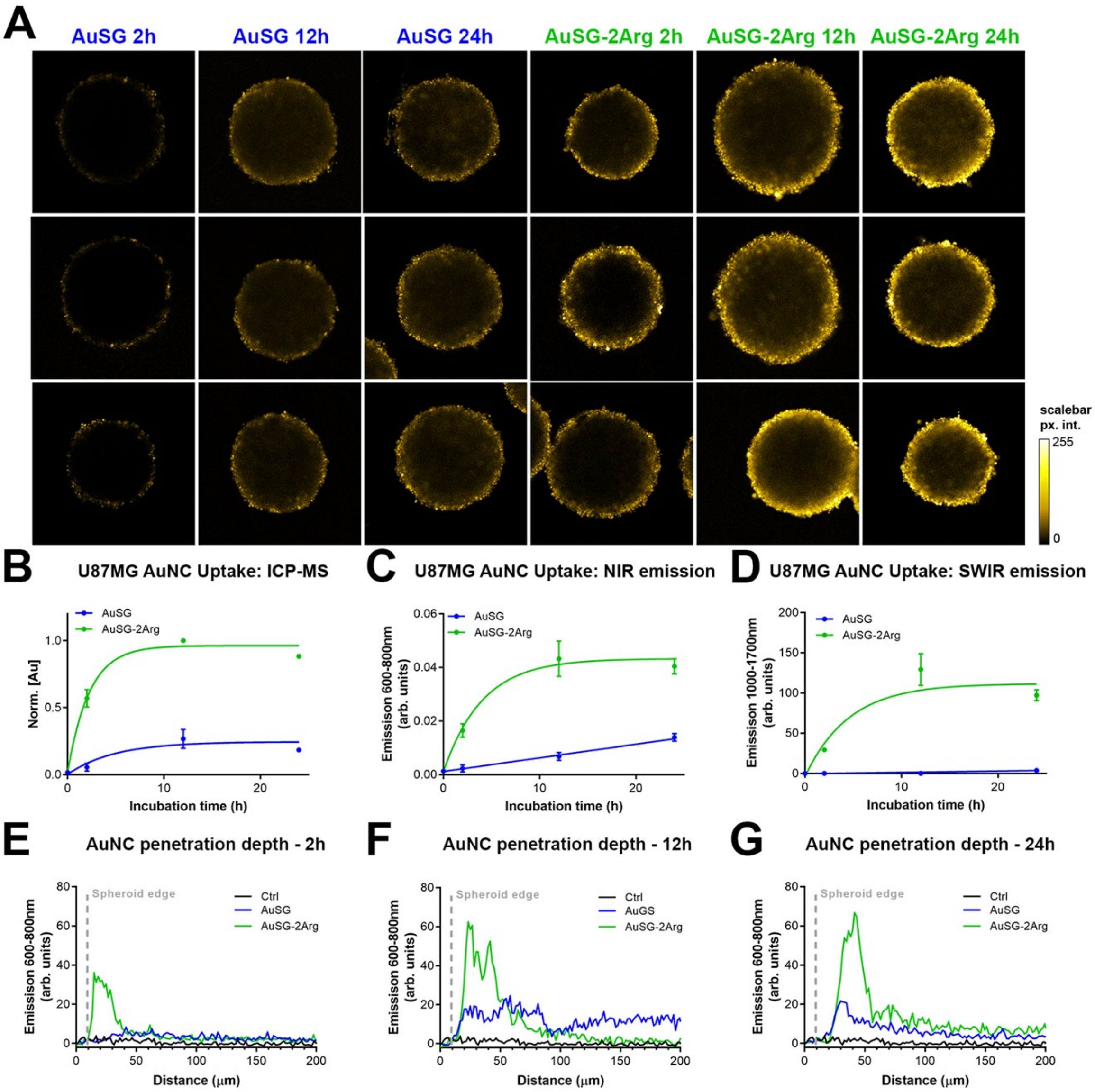

Figure S4. Arginine-functionalized gold nanoclusters are efficiently taken up by U87MG glioblastoma spheroids. (A-C) Quantification of AuNCs uptake by ICP-MS (A), NIR confocal fluorescence microscopy (B), and SWIR fluorescence macroscopy (C). (D) NIR fluorescence images of AuNCs in U87MG spheroids. AuNCs fluorescence is depicted in yellow, scalebar = 200 µm. (E-G) Fluorescence intensity profiles obtained from the radius of the spheroids. Data was acquired after a 2 h incubation (E), 12 h incubation (F), or 24 h incubation (G). ***Please note that Panels A, B, and F are also depicted in the main manuscript. The graphs are maintained here to facilitate a direct comparison with the F98 rat glioblastoma spheroids (Fig. S5)***

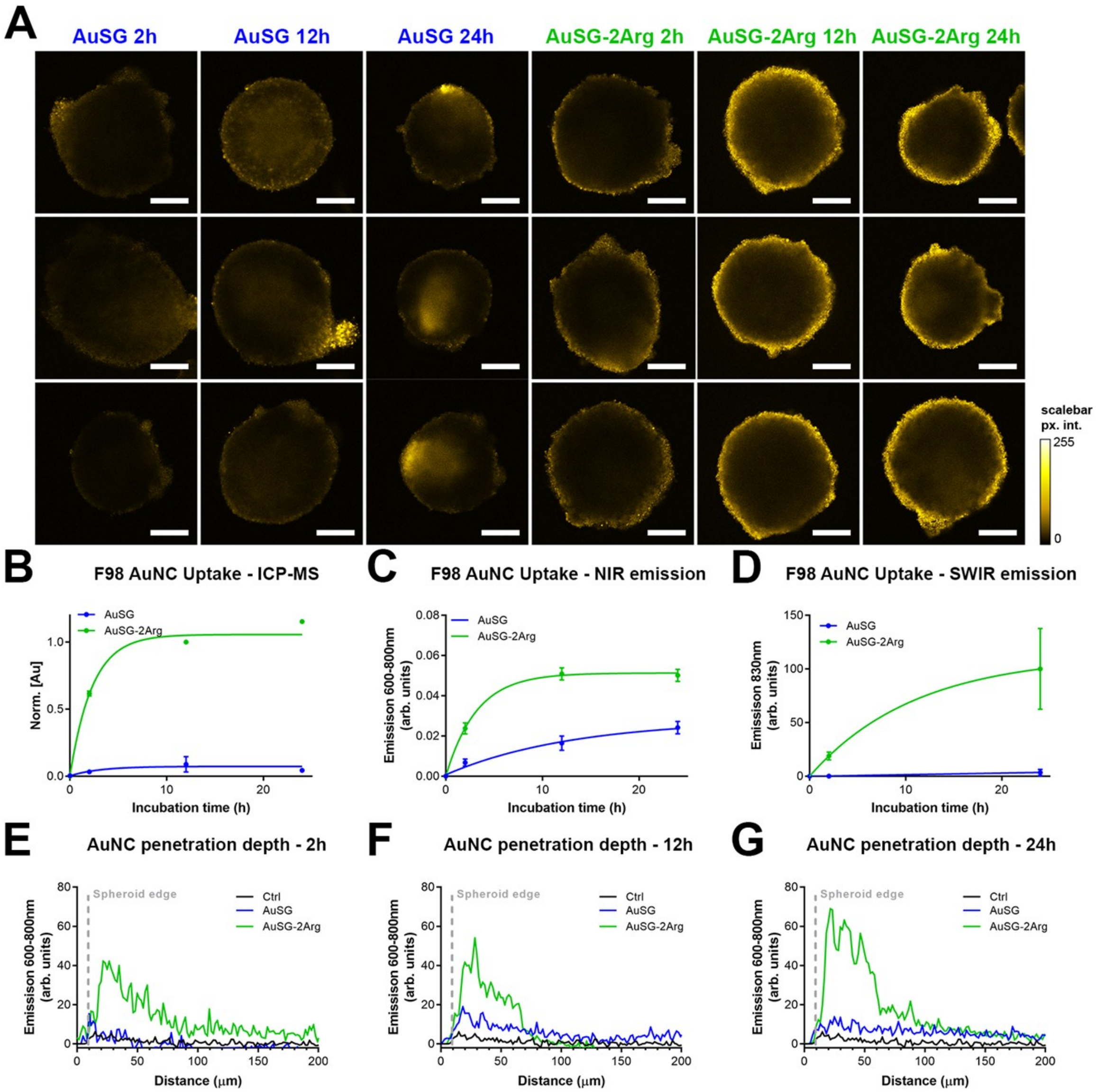

Figure S5. Arginine-functionalized gold nanoclusters are efficiently taken up by F98 glioblastoma spheroids. (A-C) Quantification of AuNCs uptake by ICP-MS (A), NIR confocal fluorescence microscopy (B), and SWIR fluorescence macroscopy (C). (D) NIR fluorescence images of AuNCs in F98 spheroids. AuNCs fluorescence is depicted in yellow, scalebar = 200 µm. (E-G) Fluorescence intensity profiles obtained from the radius of the spheroids. Data was acquired after a 2 h incubation (E), 12 h incubation (F), or 24 h incubation (G).

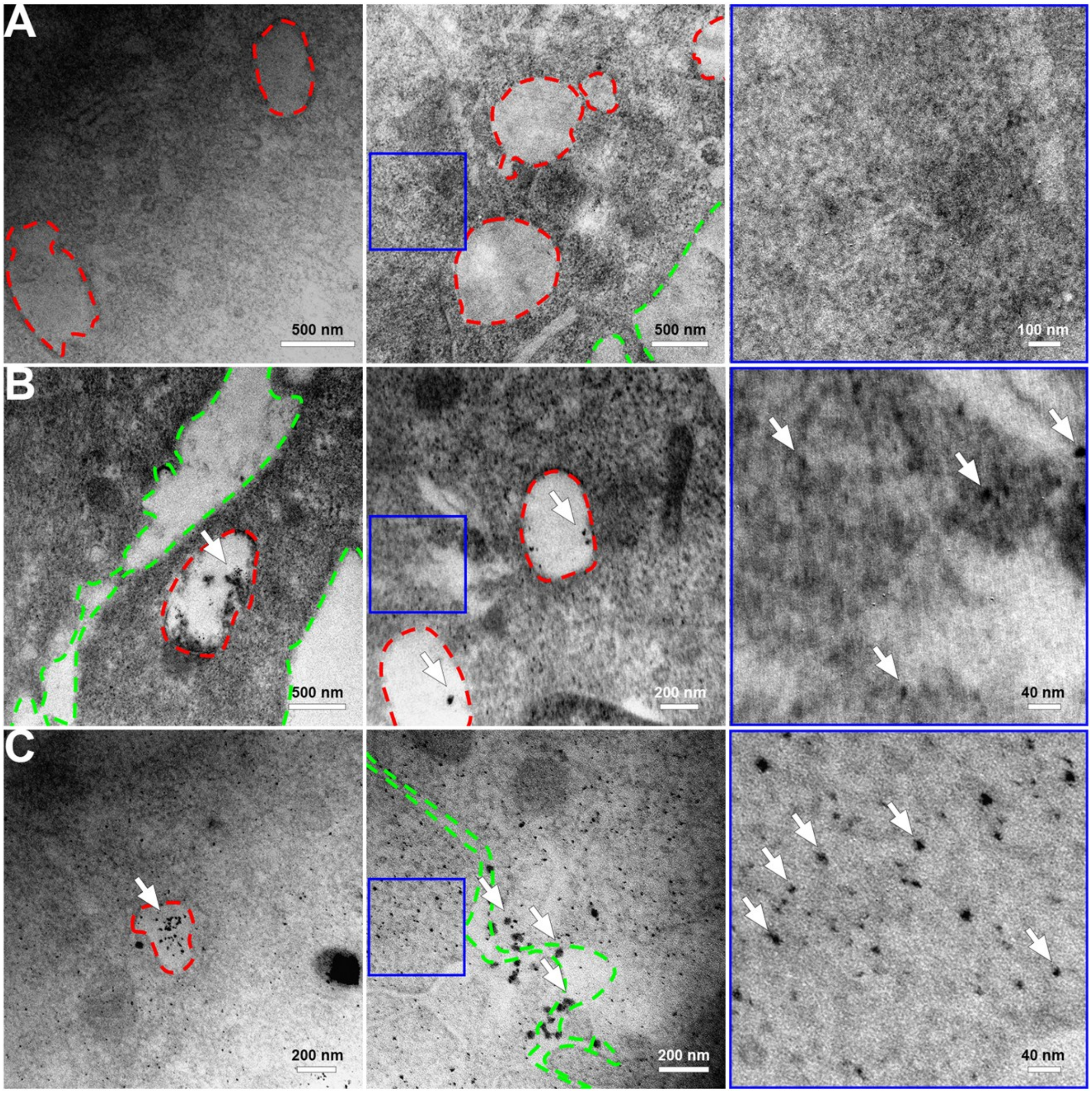

Figure S6. Investigations on AuSG and AuSG-2Arg localization in U87MG spheroids using transmission electron microscopy. Images were taken from (A) untreated spheroids, (B) AuSG-treated spheroids, and (C) AuSG-2Arg-treated spheroids. Endosomes are delineated in red, plasma membranes are outlined in green. The last image in each panel is a magnified area from the second figure as outlined in blue.

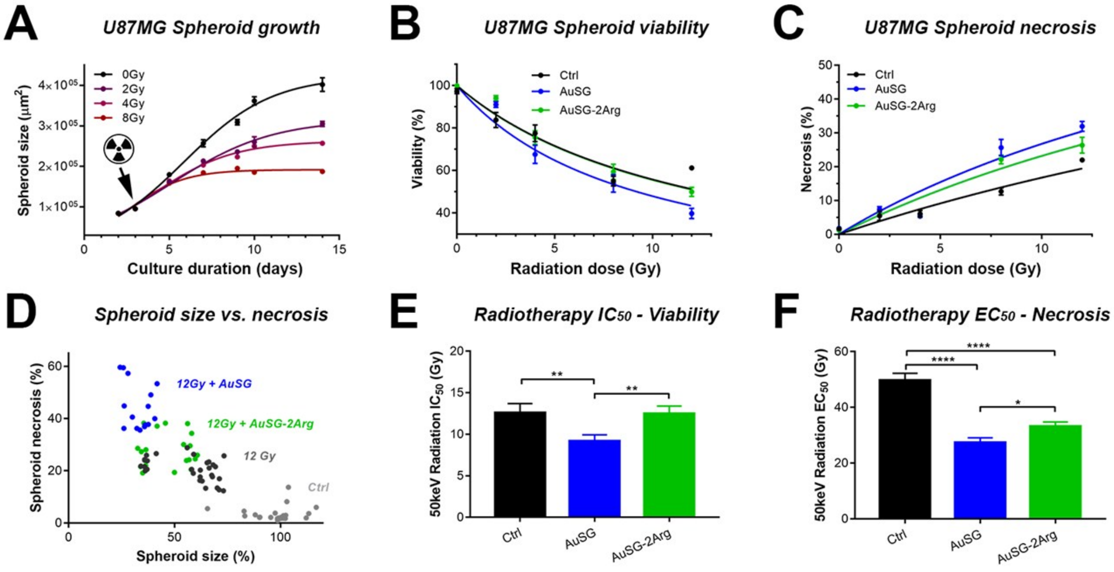

Figure S7. Extended evaluation of 50 keV radiation dose enhancement by AuNCs in U87MG glioblastoma spheroids. (A) Effect of 50 keV radiotherapy on U87MG spheroids growth (logarithmic growth fits). **(B)** Radiation dose response fits of U87MG spheroids viability following radiotherapy alone (black), radiotherapy + AuSG (blue), and radiotherapy + AuSG-2Arg (green). **(C)** Radiation dose response fits of U87MG spheroids necrosis following radiotherapy alone (black), radiotherapy + AuSG (blue), and radiotherapy + AuSG-2Arg (green). **(D)** Spheroids size plotted as a function of necrosis following no treatment (light grey), 12 Gy radiotherapy alone (dark grey), AuSG + 12 Gy (blue) and AuSG-2Arg + 12 Gy (green). **(E)** Statistical comparison (extra sum-of-squares f-test) of the fitted IC_{50} values for radiotherapy alone (black), radiotherapy + AuSG (blue), and radiotherapy + AuSG-2Arg (green). **(F)** Statistical comparison (extra sum-of-squares f-test) of the fitted EC_{50} values for radiotherapy alone (black), radiotherapy + AuSG (blue), and radiotherapy + AuSG-2Arg (green), based on treatment-induced necrosis. All data represents the mean ± SEM from N ≥ 9 obtained from 3 technical repeats. ***Please note that Panels A, and D are also depicted in the main manuscript. The graphs are maintained here to facilitate a direct comparison with the F98 rat glioblastoma spheroids (Fig. S9)***

Figure S8 (next page): Live/dead heatmaps displaying radiotherapy dose-response effects on U87MG spheroid viability. (A) Viability heatmaps of the treatment group receiving radiotherapy alone. **(B)** Viability heatmaps of the treatment group receiving radiotherapy upon AuSG treatment**. (C)** Viability heatmaps of the treatment group receiving radiotherapy upon AuSG treatment. Depicted are three representative spheroids per treatment group, from a total of N ≥ 12 derived from three technical repeats. Scalebar = 200 μm.

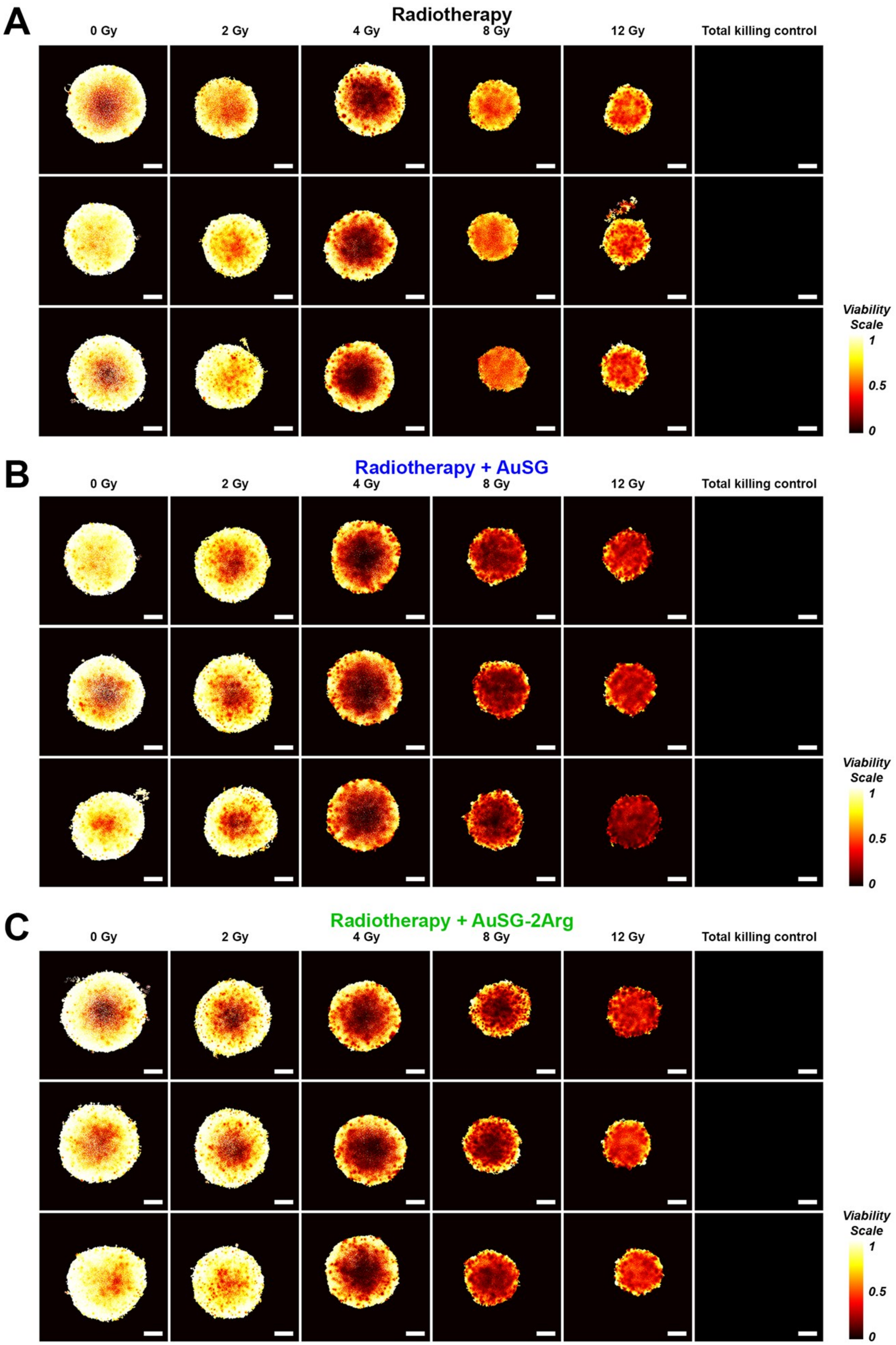
A
Radiotherapy
0 Gy
2 Gy
4 Gy
8 Gy
12 Gy
Total killing control
Viability Scale
1
0.5
0
B
Radiotherapy + AuSG
0 Gy
2 Gy
4 Gy
8 Gy
12 Gy
Total killing control
Viability Scale
1
0.5
0
C
Radiotherapy + AuSG-2Arg
0 Gy
2 Gy
4 Gy
8 Gy
12 Gy
Total killing control
Viability Scale
1
0.5
0

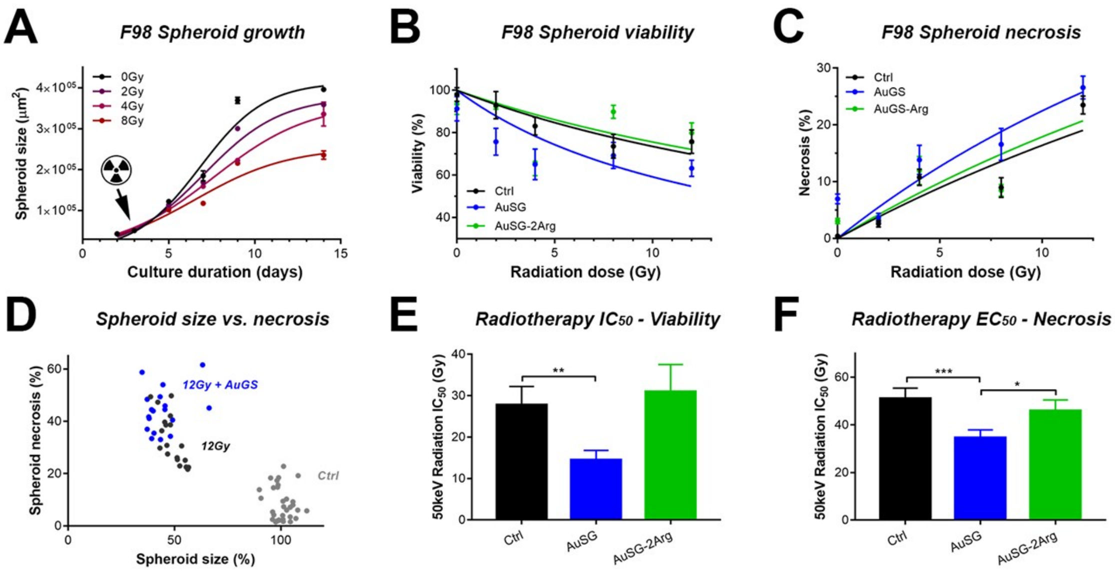

Figure S9. Multiparametric evaluation of 50 keV radiation dose enhancement by AuNCs in F98 glioblastoma spheroids. (A) Effect of 50 keV radiotherapy on F98 spheroid growth (logarithmic growth fits). **(B)** Radiation dose response fits of F98 spheroid viabilities following radiotherapy alone (black), radiotherapy + AuSG (blue), and radiotherapy + AuSG-2Arg (green). **(C)** Radiation dose response fits of F98 spheroid necrosis following radiotherapy alone (black), radiotherapy + AuSG (blue), and radiotherapy + AuSG-2Arg (green). **(D)** Spheroid size plotted as a function of spheroid necrosis following no treatment (light grey), 12 Gy radiotherapy alone (dark grey), and AuSG + 12 Gy (blue). The AuSG-2Arg + 12 Gy group was not plotted due to the overlap with the 12 Gy radiotherapy group. **(E)** Statistical comparison (extra sum-of-squares f-test) of the fitted IC_{50} values for radiotherapy alone (dark grey), AuSG + 12 Gy (blue), and radiotherapy + AuSG-2Arg (green). **(F)** Statistical comparison (extra sum-of-squares f-test) of the fitted EC_{50} values for radiotherapy alone (black), radiotherapy + AuSG (blue), and radiotherapy + AuSG-2Arg (green), based on treatment-induced necrosis. All data represent the mean ± SEM from $N \geq 9$ obtained from 3 technical repeats.

Figure S10 (next page): Live/dead heatmaps displaying radiotherapy dose-response effects on F98 spheroid viability. (A) Viability heatmaps of the treatment group receiving radiotherapy alone. **(B)** Viability heatmaps of the treatment group receiving radiotherapy upon AuSG treatment**. (C)** Viability heatmaps of the treatment group receiving radiotherapy upon AuSG treatment. Depicted are three representative spheroids per treatment group, from a total of $N \geq 12$ derived from three technical repeats. Scalebar = 200 µm.

A

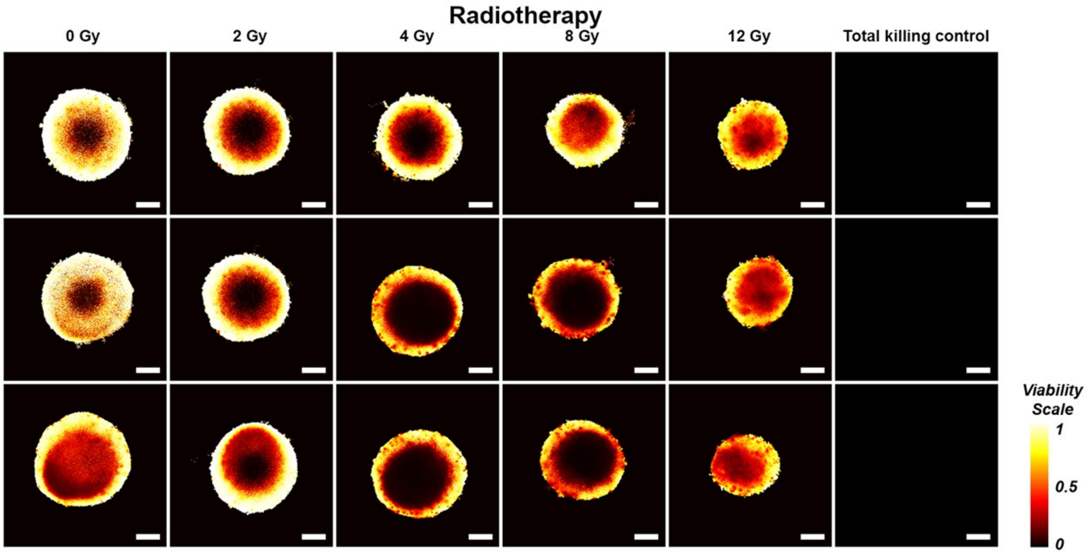
Radiotherapy
0 Gy
2 Gy
4 Gy
8 Gy
12 Gy
Total killing control
Viability Scale
1
0.5
0

B

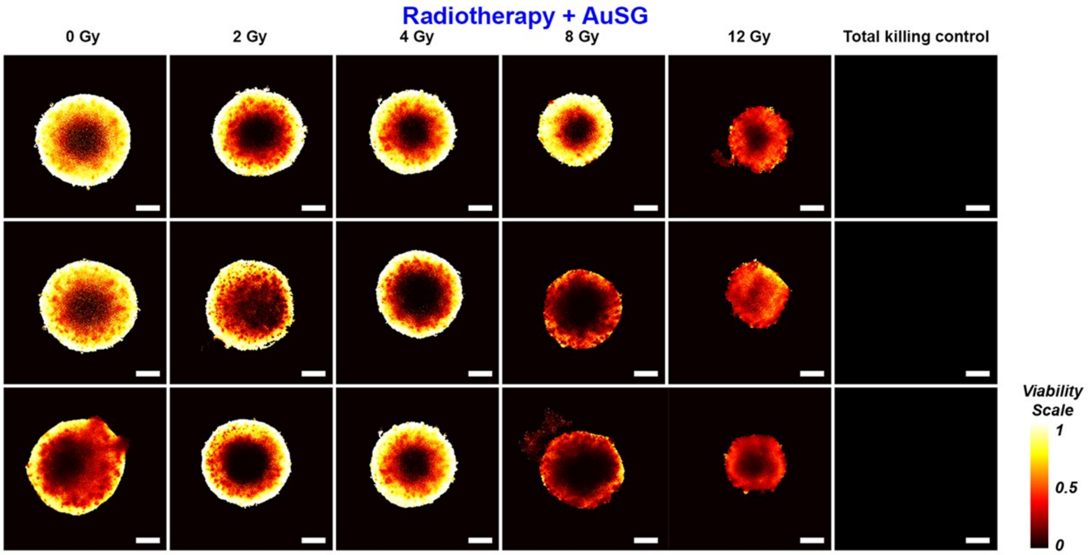
Radiotherapy + AuSG
0 Gy
2 Gy
4 Gy
8 Gy
12 Gy
Total killing control
Viability Scale
1
0.5
0

C

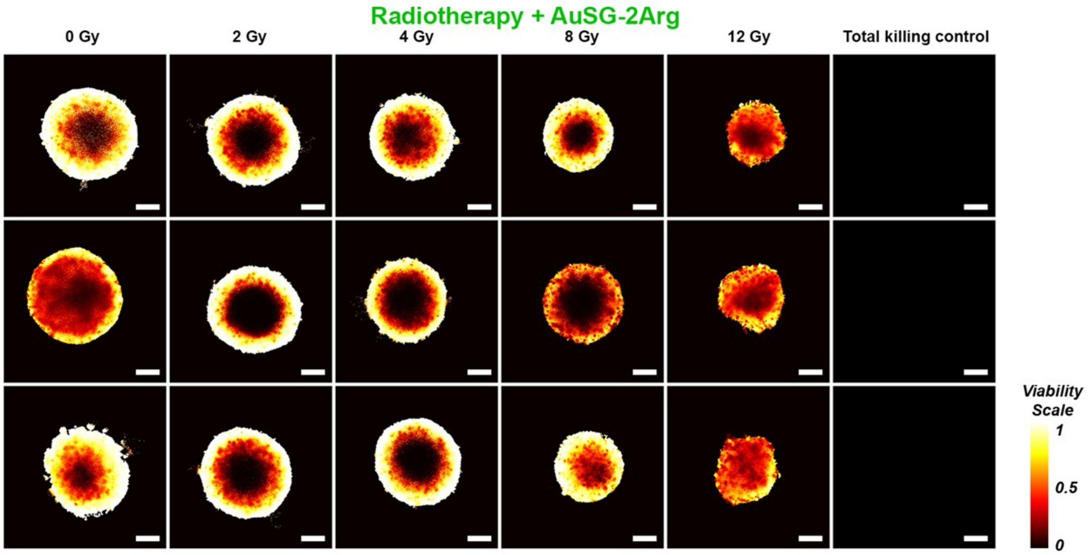
Radiotherapy + AuSG-2Arg
0 Gy
2 Gy
4 Gy
8 Gy
12 Gy
Total killing control
Viability Scale
1
0.5
0

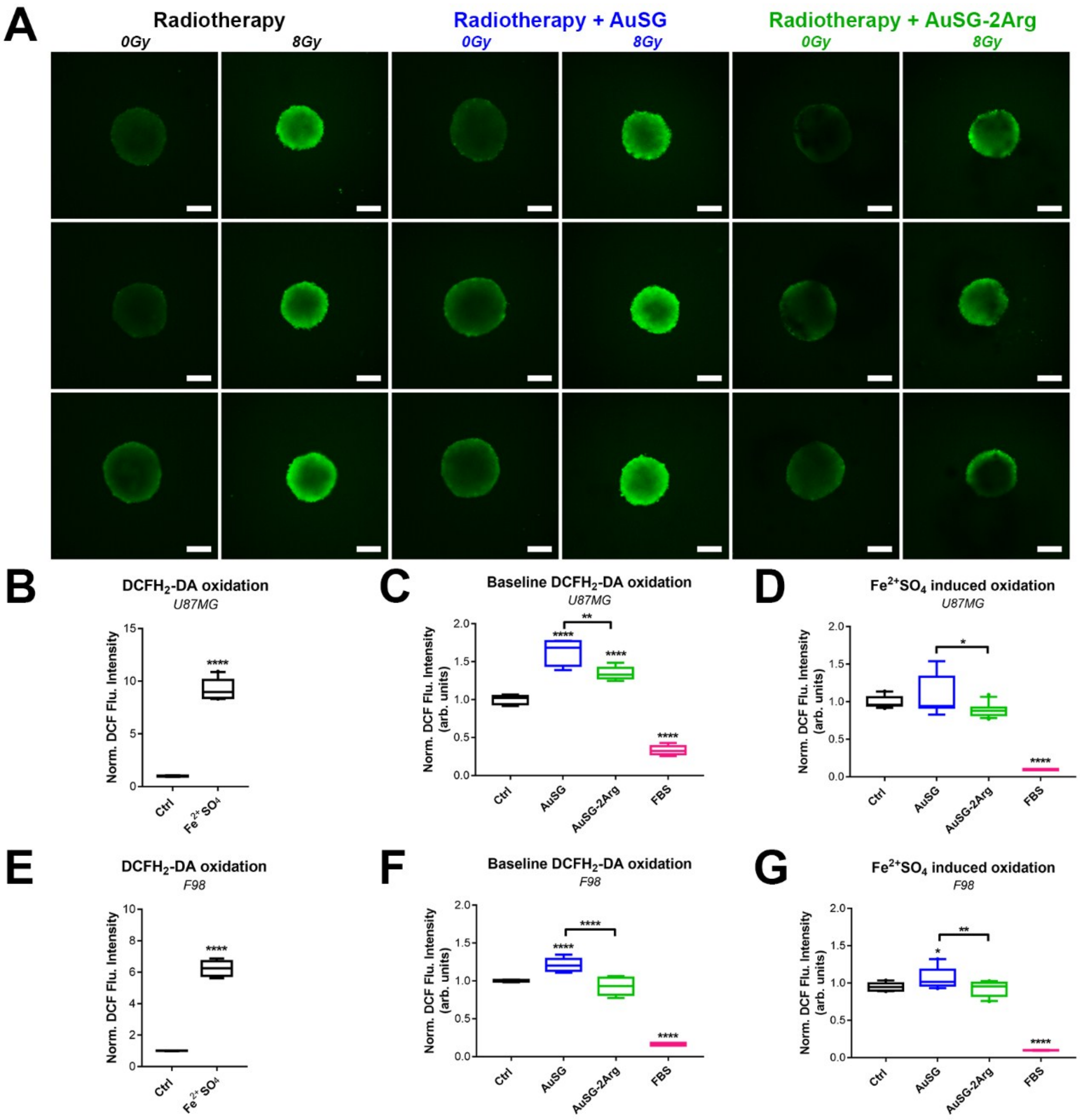

Figure S11. The effects of the AuNCs on cellular redox homeostasis and oxidative stress. (A) Supplemental DCF fluorescence microscopy images obtained from U87MG spheroids, either under untreated conditions or following exposure to radiotherapy (8 Gy). (B) Quantification of $DCFH_2$-DA oxidation in U87MG cells under non-stressed and Fe^{2+} stressed conditions. (C) $DCFH_2$-DA oxidation by non-stressed U87MG cells upon exposure to AuSG and AuSG-2Arg. (D) The effect of AuSG and AuSG-2Arg on the extent of oxidative stress in U87MG cells induced by Fe^{2+} exposure. (E) Quantification of $DCFH_2$-DA oxidation in F98 cells under non-stressed and Fe^{2+} stressed conditions. (F) $DCFH_2$-DA oxidation by non-stressed F98 cells upon exposure to AuSG and AuSG-2Arg. (G) The effect of AuSG and AuSG-2Arg on the extent of oxidative stress in F98 cells induced by Fe^{2+} exposure. All panels display the median, mean, 25th & 75th percentiles, and the 90% confidence interval of $N \geq 6$ obtained from 3 technical repeats.